








**Please cite the Published Version**

da Silveira, Andresa Rodrigues , Freire, Alisson Lopes, Elyseu, Fábio, de Fátima Peralta Muniz Moreira, Regina , Peterson, Michael , Doyle, Aidan , Pergherd, Sibebe Berenice Castella , Hotza, Dachamir  and De Noni, Agenor  (2024) Synthesis of Waste-Derived Geopolymer–Zeolite Composite with Enhanced CO<sub>2</sub> Adsorption Capacity. Eng, 5 (4). pp. 3439-3450. ISSN 2673-4117

**DOI:** <https://doi.org/10.3390/eng5040179>

**Publisher:** MDPI AG

**Version:** Published Version

**Downloaded from:** <https://e-space.mmu.ac.uk/637727/>

**Usage rights:**  [Creative Commons: Attribution 4.0](https://creativecommons.org/licenses/by/4.0/)

**Additional Information:** This is an open access article which first appeared in Eng, published by MDPI

**Data Access Statement:** More detailed data are available at <https://pergamum.ufsc.br/> accessed on 15 January 2020, searching from the master's thesis of the first author.

**Enquiries:**

If you have questions about this document, contact [openresearch@mmu.ac.uk](mailto:openresearch@mmu.ac.uk). Please include the URL of the record in e-space. If you believe that your, or a third party's rights have been compromised through this document please see our Take Down policy (available from <https://www.mmu.ac.uk/library/using-the-library/policies-and-guidelines>)

## Article

# Synthesis of Waste-Derived Geopolymer–Zeolite Composite with Enhanced CO<sub>2</sub> Adsorption Capacity

Andresa Rodrigues da Silveira <sup>1</sup>, Alisson Lopes Freire <sup>1</sup>, Fábio Elyseu <sup>2</sup>,  
Regina de Fátima Peralta Muniz Moreira <sup>1</sup>, Michael Peterson <sup>2</sup>, Aidan Doyle <sup>3</sup>,  
Sibele Berenice Castella Pergher <sup>4</sup>, Dachamir Hotza <sup>1</sup> and Agenor De Noni, Jr. <sup>1,\*</sup>

- <sup>1</sup> Department of Chemical and Food Engineering (EQA), Federal University of Santa Catarina (UFSC), Florianópolis 888037-110, SC, Brazil; rodrigues.andresa@hotmail.com (A.R.d.S.); freire.alisson@hotmail.com (A.L.F.); regina.moreira@ufsc.br (R.d.F.P.M.M.); d.hotza@ufsc.br (D.H.)
- <sup>2</sup> Graduate Program in Materials Science and Engineering, University of the Extreme South of Santa Catarina, Criciúma 88806-000, SC, Brazil; labvalora@unesoc.net (F.E.); michael@unesoc.net (M.P.)
- <sup>3</sup> Department of Natural Sciences, Manchester Metropolitan University, Manchester M15 6BH, UK; a.m.doyle@mmu.ac.uk
- <sup>4</sup> Chemistry Institute, Federal University of Rio Grande do Norte (UFRN), Natal 59078-900, RN, Brazil; sibele.pergher@ufrn.br
- \* Correspondence: agenor.junior@ufsc.br; Tel.: +55-48-3721-6340

**Abstract:** Carbon dioxide levels in the atmosphere are related to global warming and climate change. Materials to be used for CO<sub>2</sub> capture are an important factor in assisting humanity in overcoming this challenge. The goals of this study are to look into the synthesis of adsorbents from red mud (RM), fly ash (FA), and metakaolin (MK). The initial composition was chosen to induce in situ crystallization of zeolites dispersed together with a geopolymer matrix. Two aging steps were used, which combined temperature (25; 95 °C) and atmosphere (air; water). The MK + FA system crystallized zeolite sites dispersed throughout the geopolymer matrix. These crystals were identified as faujasite-Na. They were responsible for the surface area ranging from 23.2 to 238.4 m<sup>2</sup>·g<sup>-1</sup>, and CO<sub>2</sub> adsorption from 0.83 to 2.32 mmol·g<sup>-1</sup> at 35 °C and 1 atm. The best results were obtained by first aging at 95 °C for 120 h, followed by water aging at 25 °C for 120 h.

**Keywords:** red mud; metakaolin; fly ash; geopolymer; CO<sub>2</sub> capture



**Citation:** da Silveira, A.R.; Freire, A.L.; Elyseu, F.; de Fátima Peralta Muniz Moreira, R.; Peterson, M.; Doyle, A.; Pergher, S.B.C.; Hotza, D.; De Noni, A., Jr. Synthesis of Waste-Derived Geopolymer–Zeolite Composite with Enhanced CO<sub>2</sub> Adsorption Capacity. *Eng* **2024**, *5*, 3439–3450. <https://doi.org/10.3390/eng5040179>

Academic Editor: Qiuwan Shen

Received: 16 November 2024

Revised: 12 December 2024

Accepted: 16 December 2024

Published: 18 December 2024



**Copyright:** © 2024 by the authors. Licensee MDPI, Basel, Switzerland. This article is an open access article distributed under the terms and conditions of the Creative Commons Attribution (CC BY) license (<https://creativecommons.org/licenses/by/4.0/>).

## 1. Introduction

In 2023, the carbon dioxide concentration in the atmosphere increased by 419.3 parts per million [1], while CO<sub>2</sub> emissions increased by 37 billion tons. Both parameters have a very strong direct correlation. Global warming and climate change are closely related to CO<sub>2</sub> levels in the atmosphere, as well as levels of other greenhouse gases such as methane and nitrous oxide [1,2]. Reducing CO<sub>2</sub> emissions from anthropogenic activities has been identified as the most important factor in reducing or stopping global warming [3]. The 2015 United Nations Climate Change Conference, COP 21, established a goal of keeping global warming between 1.5 °C and 2 °C, in accordance with the recommendations of the Intergovernmental Panel on Climate Change (IPCC) [4]. There are two main options for achieving this goal: (1) substitution of fossil fuels by renewable fuels and (2) capture of CO<sub>2</sub> from the atmosphere. In the case of CO<sub>2</sub> capture, various materials or processes, such as membrane separation [3], and absorption [4] and adsorption technologies [5], have been used. The most common materials found to be considered in adsorptive technologies are activated carbon, amorphous silica, metalorganic compounds, and zeolites [6–10]. A new generation of nanocatalysts have also been suggested in the literature [11]. One of the main challenges is to find a feasible compromise between cost, performance, and environmental impact [5].

Some of the most promising materials to be used in this field are zeolites. Natural or synthetic, they have crystalline and microporous structures. Other features include a large surface area, thermal stability, and selectivity [10,12]. Their adsorption capacity is affected by the alkalinity, porosity, and intensity of the electric field used during adsorption [10,12]. Synthetic zeolites can be made from aluminosilicate raw materials or industrial wastes like fly ash and rice husk ash [13,14]. Because the components are less prone to react, zeolites derived from waste materials typically have lower efficiencies than those derived from raw materials [14]. Despite this disadvantage, zeolites derived from waste are less expensive.

Geopolymers are another interesting material for CO<sub>2</sub> capture. They can also be obtained from waste, and their synthesis occurs at lower temperatures and pressures than zeolites, resulting in less energy consumption [15–17]. Because of their structural, thermal, and physical properties, they have attracted the attention of researchers all over the world [18,19] due to the possibility of developing particular properties such as high compressive strength, an adsorptive capacity to remove heavy metals dissolved in water, a moisture-buffering capacity, and a CO<sub>2</sub> adsorptive capacity [20]. The properties are strongly affected by the operational conditions used in the synthesis and the composition of the raw materials [21–23]. Several solid residues containing aluminosilicates can also be incorporated, such as fly ash [24], red mud [25,26], and blast furnace slags [18], as attractive alternatives to immobilize industrial solid residues.

In general, crystalline geopolymers are produced when the Si/Al ratio is ~1, and the curing conditions are particularly important to promote crystallization. Zeolitic phases such as hydroxy-sodalite (SOD), faujasite (FAU), and Linde Type A (LTA) are among the most commonly found in geopolymerization processes. Therefore, geopolymer–zeolite composites have attracted the interest of many researchers [19,27].

The objective of this research is to investigate the synthesis of CO<sub>2</sub> adsorbents from two different types of waste, red mud and fly ash. The strategy was to increase the adsorptive capacity of zeolite sites while also increasing the mechanical strength by incorporating a geopolymer matrix. The zeolite type was not previously defined. In order to form zeolites in situ, dispersed together with a geopolymer matrix, the composition and curing conditions were established.

## 2. Materials and Methods

### 2.1. Raw Materials

Aluminosilicates were obtained from washed kaolin, fly ash (FA), and red mud (RM). Torrecid (Içara, SC, Brazil) supplied the washed kaolin. FA originated at the Jorge Lacerda thermal power plant (Capivari de Baixo, SC, Brazil). RM was obtained from the Alunorte bauxite refinery (Barcarena, PA, Brazil). The alkali activator was made up of sodium hydroxide aqueous solution (50% *w/w* NaOH) and sodium silicate aqueous solution (15.1% *w/w* Na<sub>2</sub>O and 33.2% *w/w* SiO<sub>2</sub>) supplied by Oregon Química (Içara, SC, Brazil). FA was dried and subjected to a magnetic separation before use. Kaolin and RM were dried and calcined in an air atmosphere at 800 °C for 20 min at a heating rate of 10 °C/min [16,26].

### 2.2. Raw Material Characterization

Table 1 shows the composition measured by X-ray fluorescence (XRF, Malvern Panalytical, AXIOS Max, Almelo, The Netherlands) of the materials after the aforementioned procedure. Table 1 also shows the composition taken into account for the reaction to calculate the dosage to achieve the desired stoichiometry. Calcination promotes amorphization in kaolin due to crystalline water decomposition, resulting in a so-called metakaolin (MK). In the case of RM, the literature indicates that 800 °C is high enough to decompose gibbsite, sodalite, and hydroxides [28,29], resulting in an amorphous structure with higher reactivity.

**Table 1.** Oxide composition in mass % of geopolymer precursor materials, and their respective contents when considered as the reactive part of the mixture.

Oxides	Metakaolin		Fly Ash		Red Mud	
	Total	Reactive *	Total	Reactive *	Total	Reactive **
SiO <sub>2</sub>	54.3	50.0	65.4	52.3	17.3	17.3
Al <sub>2</sub> O <sub>3</sub>	44.2	44.2	24.6	14.5	22.1	22.1
Na <sub>2</sub> O	-	-	0.5	0.5	9.7	9.7
Fe <sub>2</sub> O <sub>3</sub>	0.3		2.6		37.3	
K <sub>2</sub> O	1.0		2.8		0.1	
CaO	-		1.4		1.2	
MgO	-		1.2		0.05	
TiO <sub>2</sub>	-		1.0		6.8	
SO <sub>3</sub>	-		0.5		-	
P <sub>2</sub> O <sub>5</sub>	-		-		-	
MnO	-		-		0.1	
L.O.I	0.2		1.0		-	
Others					5.3	
Total	100		100		100	

\* Quantification by extraction/alkaline reaction [12]. - Trace/not determined; \*\* assumed as reactive for dosage.

Scanning electron microscopy (SEM, Hitachi, TM3030, Tokyo, Japan) and X-ray diffraction (XRD, Rigaku, MiniFlex600, Tokyo, Japan, Cu K $\alpha$  radiation, from 3° to 80°) were used to characterize the raw materials. The particle size distribution was determined in a liquid medium by laser diffraction (Cilas 1064, Orleans, France). Particle sizes smaller than 45  $\mu$ m are within the expected range for geopolymers to have satisfactory strength and workability [24].

### 2.3. Geopolymer Synthesis

Table 2 shows the composition of the raw material in terms of reactive oxides and mass dosages. The ternary diagram in Figure 1 depicts the oxide composition of all materials based on reactive oxides. The compositional intervals proposed by Davidovits et al. [30] are represented by gray dashed lines, with the intersection region represented by a 4-sided polygon. It was found that the planned geopolymer dosage exceeds the suggested limits. This displacement in the direction of the greatest amount of Na<sub>2</sub>O was chosen to shift the equilibrium toward the formation of zeolitic structures in the geopolymer matrix.

**Table 2.** Composition in oxides and mass percentage values of the materials used.

Components	SiO <sub>2</sub>	Al <sub>2</sub> O <sub>3</sub>	Na <sub>2</sub> O	H <sub>2</sub> O
Mass fraction	0.535	0.224	0.241	0.589 * 0.462 **
Molar fraction	0.595	0.146	0.259	2.19 * 1.71 **
Ratio	Na <sub>2</sub> O/SiO <sub>2</sub>	SiO <sub>2</sub> /Al <sub>2</sub> O <sub>3</sub>	Na <sub>2</sub> O/Al <sub>2</sub> O <sub>3</sub>	H <sub>2</sub> O/Na <sub>2</sub> O
Molar ratio	0.43	4.1	1.8	8.4 * 6.6 **
Raw materials	RM or MK (%)	FA (%)	NaOH <sub>aq</sub>	SS <sub>aq</sub>
MK + FA	28.7	23.5	32.4	15.4
RM + FA	36.1	34.9	19.6	9.4

\* MK + FA system, \*\* RM + FA system.

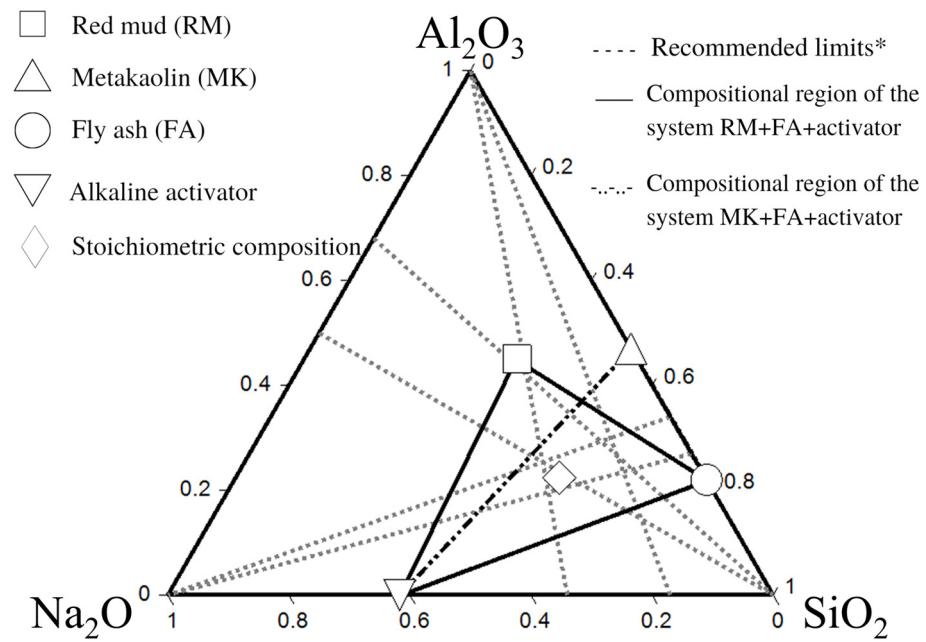


Figure 1. Ternary diagram to obtain the mass percentages of geopolymers. \* Davidovits et al. [30].

The composition was set outside of the recommended limits for structural applications where high mechanical strength is the most important feature. The goal was to shift the reaction equilibrium and induce crystallization of zeolite sites to increase surface area and thus CO<sub>2</sub> adsorption.

Figure 2 is a flowchart representing the process and general conditions applied to obtain the geopolymer samples. After the curing time, the samples were demolded and sealed with a polymeric thin film for the Aging 1 step. The film used in Aging 1 was removed for Aging 2. All experimental runs and labels are listed in Table 3.

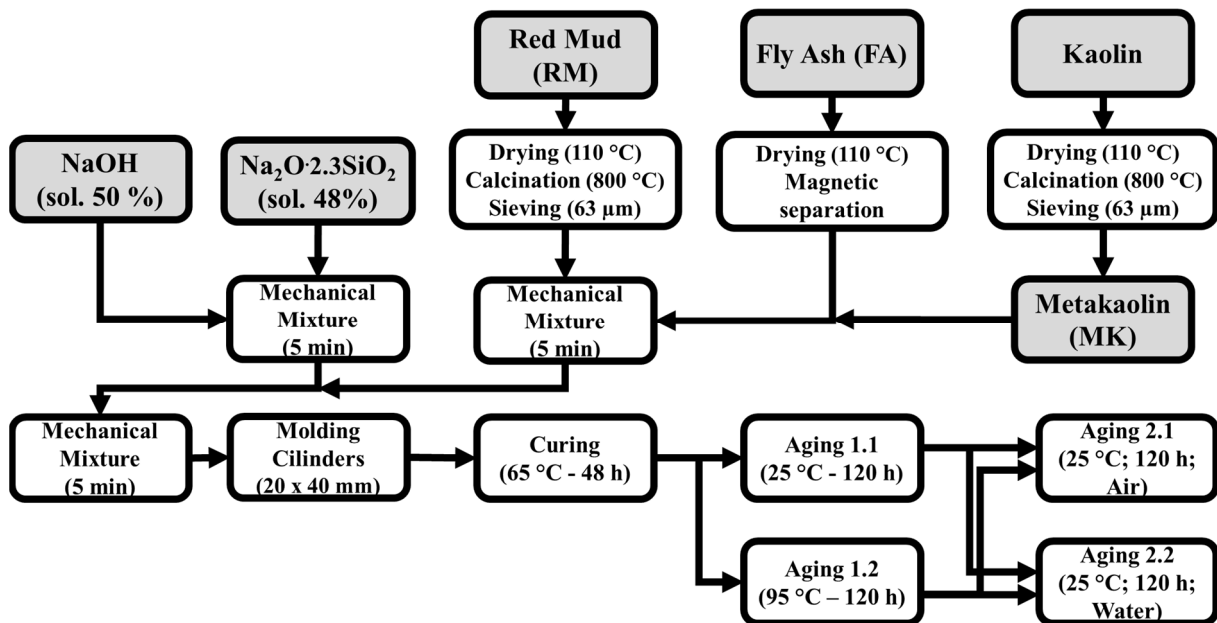


Figure 2. Flowchart of geopolymer preparation.

**Table 3.** Curing conditions of geopolymer materials.

Run	Label	Raw Materials	Curing	Aging 1		Aging 2	
			65 °C 48 h	25 °C 120 h	95 °C 120 h	Air 120 h	H <sub>2</sub> O 120 h
1	MK-25-Air	MK + FA	x	x		x	
2	MK-25-Wat	MK + FA	x	x			X
3	MK-95-Air	MK + FA	x		x	x	
4	MK-95-Wat	MK + FA	x		x		X
5	RM-25-Air	RM + FA	x	x		x	
6	RM-25-Wat	RM + FA	x	x			X
7	RM-95-Air	RM + FA	x		x	x	
8	RM-95-Wat	RM + FA	x		x		X

#### 2.4. Geopolymer Characterization

XRD was used to determine the qualitative mineralogical composition of the geopolymers. SEM was applied to examine the morphology. A universal testing machine (EMIC, DL10000, 100 kN, Sao Jose dos Pinhais, Brazil) was employed to measure compressive strength at a load application rate of 1 mm/min. The pressure range  $PP_0$  from 0.05 to 0.3 was used to calculate a specific surface area based on the method of Brunauer–Emmett–Teller (BET) (Nova 1200e, Quantachrome, Boynton Beach, FL, USA).

The CO<sub>2</sub> adsorption test was carried out on powder samples using a thermogravimetric analyzer (Netzsch, STA-449 F3, Selb, Germany). The material was subjected to a pretreatment under N<sub>2</sub> atmosphere (flow rate of 50 mL.min<sup>-1</sup> for 180 min at 320 °C) to remove moisture and other adsorbed gases. The CO<sub>2</sub> adsorption occurred with a flow of 80 mL.min<sup>-1</sup> and 99% purity, under isothermal conditions at 35 °C and atmospheric pressure, reproducing the conditions reported in the literature [16]. Finally, a CO<sub>2</sub> desorption step was performed for 60 min at 320 °C and an N<sub>2</sub> flow rate of 50 mL.min<sup>-1</sup>. Near-equilibrium conditions were used to calculate adsorption mass values.

### 3. Results and Discussion

#### 3.1. Characterization of Raw Materials

##### 3.1.1. Raw Material Structure

It is critical for geopolymerization that the materials have an amorphous structure, which is the starting point for the reactions [31–33]. Amorphous-rich materials such as fly ash (FA) and metakaolin (MK) are well known. According to the results shown in Table 1, FA contains ~67.3% amorphous phases, while MK is ~94.2% amorphous. The XRD patterns of FA, MK, RM, and calcined RM are shown in Figure 3. Quartz (SiO<sub>2</sub>—03-065-0466) and mullite (Al(Al<sub>1,83</sub>Si<sub>1,08</sub>O<sub>4,85</sub>), 01-089-2645) were the crystalline phases found in FA. Quartz was the only crystalline phase identified in MK. The presence of a large number of crystalline phases is observed in RM: hematite (Fe<sub>2</sub>O<sub>3</sub>—01-089-8404); sodalite ((Na<sub>8</sub>(Al<sub>6</sub>Si<sub>6</sub>O<sub>24</sub>)·H<sub>2</sub>O), 00-038-0515); gibbsite (Al(OH)<sub>3</sub>—33-0018); anatase (TiO<sub>2</sub>—21-1272); and calcite (Mg<sub>0,1</sub>Ca<sub>0,9</sub>CO<sub>3</sub>—01-071-1663). From the standard composition of each phase, a rational analysis results in an approximate mass composition of 37% hematite, 39% sodalite, 10% gibbsite, and 7% anatase, with a total amount of crystalline phases of ~93%. The low intensity of the sodalite peak indicates that this phase has a low crystallization level. The decomposition of gibbsite, anatase, and calcite can be seen after calcination. Furthermore, a quartz peak was also observed; quartz was most likely formed from an amorphous phase present in RM. These findings point to an increase in RM crystallization after calcination under the conditions used.





### 3.2. Geopolymer Characterization

#### 3.2.1. Geopolymer Structure

Figure 5 depicts the obtained XRD pattern for all geopolymer compositions and aging conditions. Geopolymers are amorphous structures that are primarily formed from aluminosilicate sources [33,34]. The crystalline phases found in geopolymers are typically leftover from the raw materials. This is true for quartz and mullite in all geopolymers. Figure 5b shows the hematite and sodalite in geopolymers derived from RM + FA. The presence of mullite, calcite, and zeolites in the geopolymers derived from MK and FA has also been reported in the literature [37].

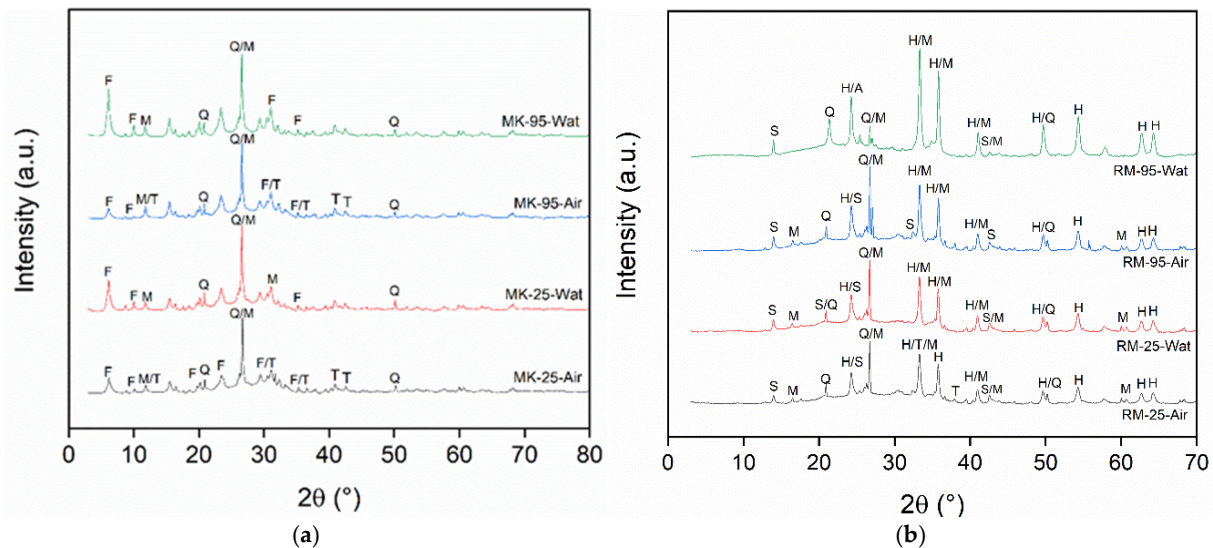


**Figure 5.** XRD patterns of geopolymers. Q: quartz; M: mullite; H: hematite; S: sodalite; F: faujasite-Na; T: thermonatrite. (a) Metakaolin-based compound; (b) red mud-based compound.

Figure 5 also depicts the formation of new phases in various compositions and aging conditions. In the case of MK + FA geopolymers, new zeolite phases could be identified. According to preliminary identification, such phases are primarily made up of a Na-faujasite structure, which is most likely a combination of faujasite-Na (zeolite Y) ( $\text{Na}_{2.06}\text{Al}_2\text{Si}_{3.8}\text{O}_{11.63}\cdot 8\text{H}_2\text{O}$ —00-038-0240), faujasite-Na (zeolite X) ( $\text{Na}_{4.43}\text{Al}_6\text{Si}_6\text{O}_{24}(\text{H}_2\text{O})_{8.882}$ —01-072-2421), faujasite-Na ( $\text{Na}_2\text{Al}_2\text{Si}_{2.4}\text{O}_{8.8}\cdot 6.7\text{H}_2\text{O}$ —00-012-0246), and zeolite X ( $\text{Na}_2\text{Al}_2\text{Si}_{2.5}\text{O}_9\cdot 6.2\text{H}_2\text{O}$ —00-038-02437). Faujasites are classified into two groups: X and Y. Group X has a Si/Al ratio of 1.0 to 1.5, while Group Y has a Si/Al ratio greater than 1.5 [38].

The intensity of the lower angle diffraction of faujasite observed in Figure 5a was higher in the water-aged samples than in the air-aged samples. Aging 1 at 95 °C produces a higher peak intensity than aging at 25 °C. This effect could be attributed to increased ionic diffusion in the presence of water and at higher temperatures. Thermonatrite ( $\text{Na}_2\text{CO}_3\cdot\text{H}_2\text{O}$ ) was also found in low concentrations, most likely as a result of an excess of NaOH in the system.

Only at 95 °C and after water aging could a difference in the geopolymer derived from RM + FA be observed. Figure 5b depicts an apparent increase in the intensity of sodalite and a strong reduction in quartz. This finding emphasizes the importance of the aging condition in the formation of structural changes.

#### 3.2.2. Geopolymer Microstructure

Figure 6 depicts the microstructure of the samples. The gel matrix formed by the geopolymer structure can be identified in all conditions. In each case, there are some unreacted particles as well. Geopolymers frequently correspond to this composite microstructure [35]. Unreacted particles are used as fillers and can provide some reinforcement [39].



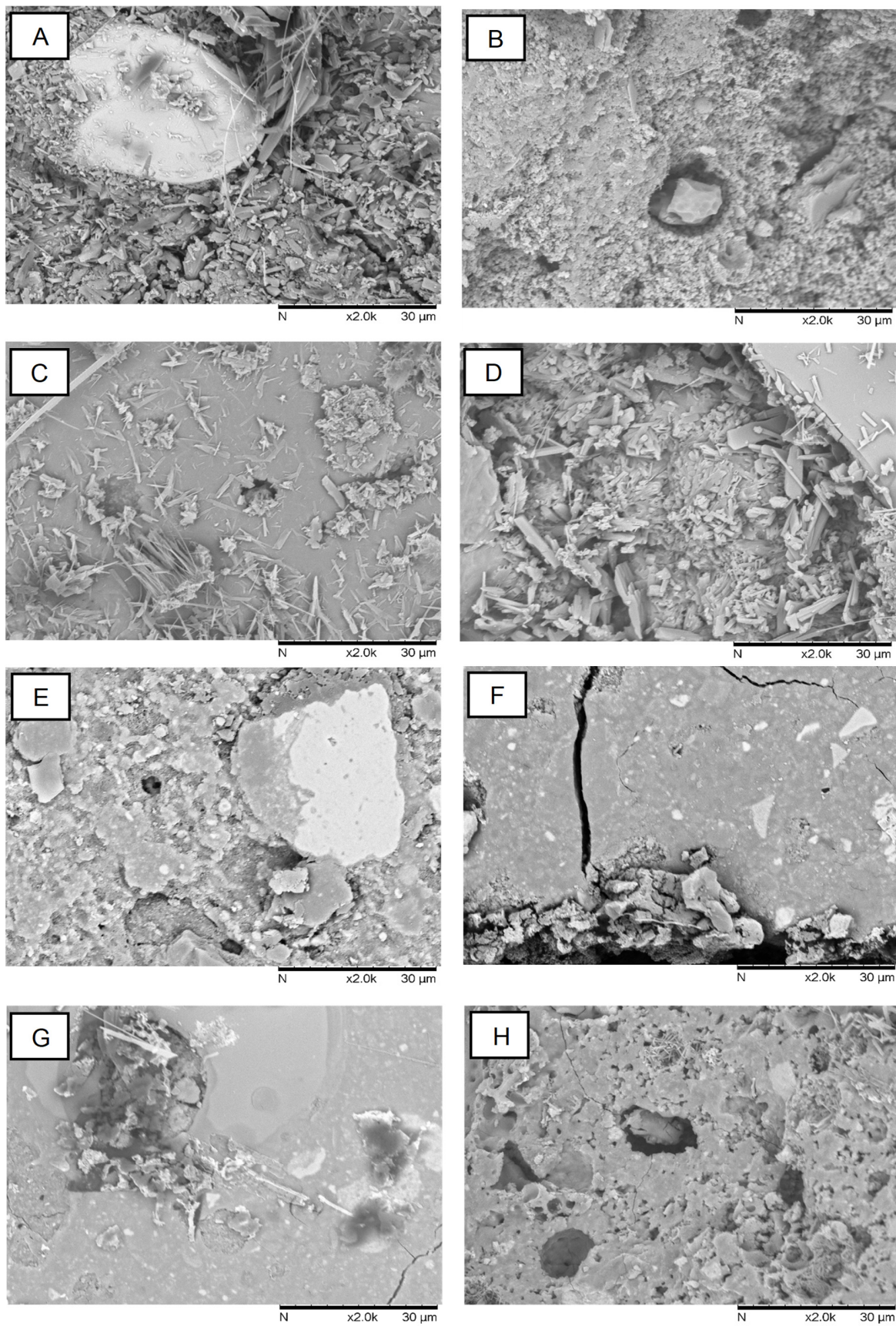


**Figure 6.** SEM morphology of geopolymers: (A) MK-25-Air; (B) MK-25-Wat; (C) MK-95-Air; (D) MK-95-Water; (E) RM-25-Air; (F) RM-25-Water; (G) RM-95-Air; (H) RM-95-Wat.

The microstructures were significantly influenced by the aging conditions. The highest concentrations of unreacted particles were found in the MK-FA compositions after 25 °C, followed by air exposure. Aging at 95 °C induced the formation of a denser matrix. The crystallization of faujasite particles is also visible, with concentrations higher in samples subjected to water aging at 25 and 95 °C, respectively. This agrees with the XRD findings. Unreacted RM particles are likely to remain in the RM + FA composition due to their irregular format and size distribution. By reacting with the activator, the FA particles were most likely responsible for forming the gel structure. Except for 25 °C and air, the aging conditions appear to have little effect on the microstructure. As with MK + FA, a more granular texture can be seen.

### 3.2.3. Geopolymer Properties

Table 4 shows the mechanical strength, surface area, and CO<sub>2</sub> adsorptive capacity for the materials produced in this study. First and foremost, it is critical to note the wide range of properties obtained in response to the starting material and aging conditions. Mechanical strength ranges from 0 to 11.8 MPa, surface area from 1.8 to 238.4 m<sup>2</sup>.g<sup>-1</sup>, and CO<sub>2</sub> adsorption from 0.05 to 2.32 mmol.g<sup>-1</sup>.

**Table 4.** Compression strength (CS), specific surface area (SA), CO<sub>2</sub> adsorption (CO<sub>2</sub>.Ad), and specific CO<sub>2</sub> adsorption (Sp.CO<sub>2</sub>.Ad) of the geopolymer specimens as a function of curing conditions and type of precursor. \* Not stable to compression.

Label	CS (MPa)	SA (m <sup>2</sup> .g <sup>-1</sup> )	CO <sub>2</sub> .Ad (mmol.g <sup>-1</sup> )	Sp.CO <sub>2</sub> .Ad (μmol.m <sup>-2</sup> )
MK-25-Air	11.8 ± 2.1	31.0	0.83	27
MK-25-Wat	7.5 ± 1.3	99.0	1.48	15
MK-95-Air	6.7 ± 1.4	23.2	1.29	55
MK-95-Wat	7.6 ± 1.4	238.4	2.32	10
RM-25-Air	8.9 ± 0.56	12.4	0.07	6
RM-25-Wat	4.7 ± 0.35	32.1	0.39	12
RM-95-Air	- *	1.8	0.05	28
RM-95-Wat	- *	3.3	0.14	42

The results of the MK + FA and RM + FA samples indicate that both compression strength and adsorption capacity are antagonistic properties. The higher mechanical strength, 11.8 and 8.9 MPa for the MK + FA and RM + FA systems, respectively, resulted in lower CO<sub>2</sub> adsorption, 0.83 and 0.07 mmol.g<sup>-1</sup>, when compared within their group. Despite this negative correlation, the literature reports that geopolymer–zeolite systems with compressive strength ranging from 3.0 to 7.5 MPa are sufficient for self-supporting monoliths [19,40]. Mechanical strength increases with low-temperature aging (25 °C) and air exposure. Because of the crystallization of zeolite phases, higher temperatures and water aging result in lower compression strength and higher adsorption capacity.

Water aging had the greatest effect on adsorption capacity in all cases. Because of the acidic nature of CO<sub>2</sub> molecules, the literature reports a positive correlation between CO<sub>2</sub> adsorptive capacity and active site basicity [16]. Water aging has increased the surface area of the MK + FA system and, thus, the CO<sub>2</sub> adsorption capacity. The specific adsorption numbers suggest a possible decrease in the basicity of the sites. Water aging caused sodium leaching, which likely reduced the sodium atoms in the zeolite framework. Water aging has increased the surface area and specific adsorption of the RM + FA system. This system's lower surface area and low reactivity could be attributed to the presence of higher crystalline phases and hematite. According to the literature, Fe ions influence the dissolution of aluminum silicates [29].

The CO<sub>2</sub> adsorption results of the geopolymer–zeolite composite can be compared to the starting materials: MK—0.33 mmol.g<sup>-1</sup>, FA—0.53 mmol.g<sup>-1</sup>, and RM—0.07 mmol.g<sup>-1</sup>. All composites resulted in higher adsorption capacity for the MK + FA system, where the

values varied between 2 and 5 times more CO<sub>2</sub> adsorbed per mass of adsorbent. These results can be attributed to the zeolite sites. The effect of the RM + FA system was the opposite: 1 to 5 times lower than the starting materials.

The findings can also be compared to those of other studies. Freire et al. [16] reported a higher value of 0.78 mmol.g<sup>-1</sup> of CO<sub>2</sub> adsorbed at 1 atm and 35 °C for geopolymers derived from MK and FA and 0.80 mmol.g<sup>-1</sup> for geopolymers derived from MK, FA, and rice husk ash, both with NaOH as an activator. In those cases, the mechanical strength was 11 and 3 MPa, respectively.

Minelli et al. [17] reported a higher value of 0.62 mmol.g<sup>-1</sup> for a geopolymer obtained from MK and KOH as an activator under the same adsorption conditions. According to Esteves et al. [41], activated carbon has a molarity of 1.2 mmol.g<sup>-1</sup>. Sayari and Belmabkhout [42] reported 2.6 mmol.g<sup>-1</sup> for amine-mesoporous silica in a more complex system, and Cavenati et al. [43] reported 4.0 mmol.g<sup>-1</sup> for pure zeolite 13X. In the review published recently by Zang and Wang [5], the authors have reported values from 0.08 to 4.1 mmol.g<sup>-1</sup> for the metal organic framework, 1.9–3.0 mmol.g<sup>-1</sup> for the covalent triazine framework, and ~1.3 mmol.g<sup>-1</sup> for hyper crosslinked polymers. This comparison indicates that the materials obtained in this work have an interesting balance of good performance and a simple synthesis method. Scaling up will most likely result in a low-cost material at the end of the process.

#### 4. Conclusions

A composite geopolymer + zeolite monolithic material for CO<sub>2</sub> adsorption was obtained and characterized. The starting materials were fly ash (FA), red mud (RM), and metakaolin (MK) with NaOH and sodium silicate as activators. To achieve a lower cost end-product, the use of waste material and a simple synthesis process were chosen. The starting composition was designed with an excess of the activator to induce in situ zeolite crystallization in a typical geopolymer route. Two aging steps were applied after curing to evaluate their effects on the product characteristics.

In terms of CO<sub>2</sub> adsorption and mechanical properties, the materials made from RM and FA did not perform well. The RM components Al<sub>2</sub>O<sub>3</sub>, SiO<sub>2</sub>, and Na<sub>2</sub>O do not appear to be available for a reaction with the activator and FA. The thermal treatment at 800 °C did not result in the expected increase in the amorphous phase. Other pretreatments could eventually be investigated to increase the red mud reactivity.

The materials derived from MK and FA performed well. Zeolite crystallization is caused by both the starting composition as well as aging. The dispersed faujasite-Na family was formed in the geopolymer matrix, according to the primary identification. The aging condition has a significant impact on the materials' phase, microstructure, and performance. Higher temperatures during the first and second aging steps under water resulted in a larger surface area and CO<sub>2</sub> adsorption capacity. Water aging appears to be the most important step in zeolite crystallization and growth. Compression strength decreases as the presence of zeolites increases.

All of the results obtained from the MK + FA system, ranging from 0.83 to 2.32 mmol.g<sup>-1</sup>, are interesting when compared to other adsorbent materials, particularly the simplest ones. The applied route is straightforward and can be optimized to produce higher-performance material or reduce processing time.

**Author Contributions:** Conceptualization, A.D.N.J., R.d.F.P.M.M. and D.H.; methodology, A.L.F., F.E. and M.P.; formal analysis, A.R.d.S. and A.D.N.J.; investigation, A.R.d.S.; resources, A.D.N.J.; writing—original draft preparation, A.R.d.S.; writing—review and editing, D.H., A.D. and S.B.C.P.; supervision, A.D.N.J.; funding acquisition, A.D.N.J. All authors have read and agreed to the published version of the manuscript.

**Funding:** This research was funded by the Brazilian agency CAPES/PROEX, grant number 88882.345097/2019/01 and CNPQ/Universal 423626/2016-7.

**Institutional Review Board Statement:** Not applicable.



**Informed Consent Statement:** Not applicable.

**Data Availability Statement:** More detailed data are available at <https://pergamum.ufsc.br/> accessed on 15 January 2020, searching from the master's thesis of the first author.

**Acknowledgments:** The authors acknowledge the financial support from the Coordination for the Improvement of Higher Education Personnel (CAPES), under grant number PROEX 88882.345097/2019/01, and the National Council for Scientific and Technological Development (CNPq), under grant number 423626/2016-7.

**Conflicts of Interest:** The authors declare no conflicts of interest.

## References

1. Lindsey, R. Climate Change: Atmospheric Carbon Dioxide. Available online: <https://www.climate.gov/> (accessed on 11 November 2024).
2. Roser, H.; Max, R. Atmospheric Concentrations. 2020. Available online: <https://ourworldindata.org/co2-and-greenhouse-gas-emissions> (accessed on 11 November 2024).
3. Khalilpour, R.; Mumford, K.; Zhai, H.; Abbas, A.; Stevens, G.; Rubin, E.S. Membrane-based carbon capture from flue gas: A review. *J. Clean. Prod.* **2015**, *103*, 286–300. [[CrossRef](#)]
4. Alivand, M.S.; Mazaheri, O.; Wu, Y.; Stevens, G.W.; Scholes, C.A.; Mumford, K.A. Catalytic Solvent Regeneration for Energy-Efficient CO<sub>2</sub> Capture. *ACS Sustain. Chem. Eng.* **2020**, *8*, 18755–18788. [[CrossRef](#)]
5. Zhang, K.; Wang, R. A critical review on new and efficient adsorbents for CO<sub>2</sub> capture. *Chem. Eng. J.* **2024**, *485*, 149495. [[CrossRef](#)]
6. Sifat, N.S.; Haseli, Y. A Critical Review of CO<sub>2</sub> Capture Technologies and Prospects for Clean Power Generation. *Energies* **2019**, *12*, 4143. [[CrossRef](#)]
7. Koysoumpa, E.I.; Bergins, C.; Kakaras, E. The CO<sub>2</sub> economy: Review of CO<sub>2</sub> capture and reuse technologies. *J. Supercrit. Fluids* **2018**, *132*, 3–16. [[CrossRef](#)]
8. Chan, W.H.; Mazlee, M.N.; Ahmad, Z.A.; Ishak, M.A.M.; Shamsul, J.B. The development of low cost adsorbents from clay and waste materials: A review. *J. Mater. Cycles Waste Manag.* **2017**, *19*, 1–14. [[CrossRef](#)]
9. Azmi, A.A.; Aziz, M.A.A. Mesoporous adsorbent for CO<sub>2</sub> capture application under mild condition: A review. *J. Environ. Chem. Eng.* **2019**, *7*, 103022. [[CrossRef](#)]
10. Nie, L.; Mu, Y.; Jin, J.; Chen, J.; Mi, J. Recent developments and consideration issues in solid adsorbents for CO<sub>2</sub> capture from flue gas. *Chin. J. Chem. Eng.* **2018**, *26*, 2303–2317. [[CrossRef](#)]
11. Alivand, M.S.; Mazaheri, O.; Wu, Y.; Zavabeti, A.; Christofferson, A.J.; Meftahi, N.; Russo, S.P.; Stevens, G.W.; Scholes, C.A.; Mumford, K.A. Engineered assembly of water-dispersible nanocatalysts enables low-cost and green CO<sub>2</sub> capture. *Nat. Commun.* **2022**, *13*, 1249. [[CrossRef](#)]
12. Wang, Q.; Luo, J.; Zhong, Z.; Borgna, A. CO<sub>2</sub> capture by solid adsorbents and their applications: Current status and new trends. *Energy Environ. Sci.* **2011**, *4*, 42–55. [[CrossRef](#)]
13. Yao, G.; Lei, J.; Zhang, X.; Sun, Z.; Zheng, S.; Komarneni, S. Mechanism of zeolite X crystallization from diatomite. *Mater. Res. Bull.* **2018**, *107*, 132–138. [[CrossRef](#)]
14. Kuroki, S.; Hashishin, T.; Morikawa, T.; Yamashita, K.; Matsuda, M. Selective synthesis of zeolites A and X from two industrial wastes: Crushed stone powder and aluminum ash. *J. Environ. Manag.* **2019**, *231*, 749–756. [[CrossRef](#)] [[PubMed](#)]
15. Chindaprasirt, P.; Rattanasak, U. Characterization of porous alkali-activated fly ash composite as a solid adsorbent. *Int. J. Greenh. Gas Control* **2019**, *85*, 30–35. [[CrossRef](#)]
16. Freire, A.L.; Moura-Nickel, C.D.; Scaratti, G.; De Rossi, A.; Araújo, M.H.; Júnior, A.D.N.; Rodrigues, A.E.; Castellón, E.R.; Moreira, R.d.F.P.M. Geopolymers produced with fly ash and rice husk ash applied to CO<sub>2</sub> capture. *J. Clean. Prod.* **2020**, *273*, 122917. [[CrossRef](#)]
17. Minelli, M.; Medri, V.; Papa, E.; Miccio, F.; Landi, E.; Doghieri, F. Geopolymers as solid adsorbent for CO<sub>2</sub> capture. *Chem. Eng. Sci.* **2016**, *148*, 267–274. [[CrossRef](#)]
18. Lemougna, P.N.; Wang, K.-T.; Tang, Q.; Cui, X.-M. Study on the development of inorganic polymers from red mud and slag system: Application in mortar and lightweight materials. *Constr. Build. Mater.* **2017**, *156*, 486–495. [[CrossRef](#)]
19. Rožek, P.; Król, M.; Mozgawa, W. Geopolymer-zeolite composites: A review. *J. Clean. Prod.* **2019**, *230*, 557–579. [[CrossRef](#)]
20. Rasaki, S.A.; Bingxue, Z.; Guarecuco, R.; Thomas, T.; Minghui, Y. Geopolymer for use in heavy metals adsorption, and advanced oxidative processes: A critical review. *J. Clean. Prod.* **2019**, *213*, 42–58. [[CrossRef](#)]
21. Davidovits, J. 30 Years of Successes and Failures in Geopolymer Applications. Market Trends and Potential Breakthroughs. In Proceedings of the Geopolymer 2002 Conference, Melbourne, Australia, 28–29 October 2002; pp. 1–16. Available online: <https://www.geopolymer.org/wp-content/uploads/30YearsGEOP.pdf> (accessed on 11 November 2024).
22. Yuan, J.; He, P.; Jia, D.; Yang, C.; Zhang, Y.; Yan, S.; Yang, Z.; Duan, X.; Wang, S.; Zhou, Y. Effect of curing temperature and SiO<sub>2</sub>/K<sub>2</sub>O molar ratio on the performance of metakaolin-based geopolymers. *Ceram. Int.* **2016**, *42*, 16184–16190. [[CrossRef](#)]
23. Duxson, P.; Fernández-Jiménez, A.; Provis, J.L.; Lukey, G.C.; Palomo, A.; van Deventer, J.S.J. Geopolymer technology: The current state of the art. *J. Mater. Sci.* **2007**, *42*, 2917–2933. [[CrossRef](#)]

24. Ascensão, G.; Seabra, M.P.; Aguiar, J.B.; Labrincha, J.A. Red mud-based geopolymers with tailored alkali diffusion properties and pH buffering ability. *J. Clean. Prod.* **2017**, *148*, 23–30. [[CrossRef](#)]
25. Chen, X.; Guo, Y.; Ding, S.; Zhang, H.Y.; Xia, F.Y.; Wang, J.; Zhou, M. Utilization of red mud in geopolymer-based pervious concrete with function of adsorption of heavy metal ions. *J. Clean. Prod.* **2019**, *207*, 789–800. [[CrossRef](#)]
26. Kaya, K.; Soyer-uzun, S. Evolution of structural characteristics and compressive strength in red mud—Metakaolin based geopolymer systems. *Ceram. Int.* **2016**, *42*, 7406–7413. [[CrossRef](#)]
27. Schneider, M.; Rodríguez-Castellón, E.; Guerrero-Pérez, M.O.; Hotza, D.; De Noni, A., Jr.; Moreira, R.F.P.M. Advances in electrospun composite polymer/zeolite and geopolymer nanofibers: A comprehensive review. *Sep. Purif. Technol.* **2024**, *340*, 126684. [[CrossRef](#)]
28. Ye, N.; Chen, Y.; Yang, J.; Liang, S.; Hu, Y.; Hu, J.; Zhu, S.; Fan, W.; Xiao, B. Transformations of Na, Al, Si and Fe species in red mud during synthesis of one-part geopolymers. *Cem. Concr. Res.* **2017**, *101*, 123–130. [[CrossRef](#)]
29. Ye, N.; Yang, J.; Ke, X.; Zhu, J.; Li, Y.; Xiang, C.; Wang, H.; Li, L.; Xiao, B. Synthesis and Characterization of Geopolymer from Bayer Red Mud with Thermal Pretreatment. *J. Am. Ceram. Soc.* **2014**, *97*, 1652–1660. [[CrossRef](#)]
30. Davidovits, J.; Davidovics, M.; Davidovits, N. Process for Obtaining a Geopolymericalumino-Silicate and Products thus Obtained. United States Patent 5,342,595, 30 August 1994.
31. Davidovits, J. Geopolymers: Ceramic-Like Inorganic Polymers. *J. Ceram. Sci. Technol.* **2017**, *8*, 335–350. [[CrossRef](#)]
32. Jian, H.; Jie, Y.; Zhang, J.; Yu, Y.; Zhang, G. Synthesis and characterization of red mud and rice husk ash-based geopolymer composites. *Cem. Concr. Compos.* **2013**, *37*, 108–118. [[CrossRef](#)]
33. He, J.; Zhang, J.; Yu, Y.; Zhang, G. The strength and microstructure of two geopolymers derived from metakaolin and red mud-fly ash admixture: A comparative study. *Constr. Build. Mater.* **2012**, *30*, 80–91. [[CrossRef](#)]
34. Hu, W.; Nie, Q.; Huang, B.; Shu, X.; He, Q. Mechanical and microstructural characterization of geopolymers derived from red mud and fly ashes. *J. Clean. Prod.* **2018**, *186*, 799–806. [[CrossRef](#)]
35. Zhang, M.; El-Korchi, T.; Zhang, G.; Liang, J.; Tao, M. Synthesis factors affecting mechanical properties, microstructure, and chemical composition of red mud–fly ash based geopolymers. *Fuel* **2014**, *134*, 315–325. [[CrossRef](#)]
36. Atasoy, A. An investigation on characterization and thermal analysis of the aughinish red mud. *J. Therm. Anal. Calorim.* **2005**, *81*, 357–361. [[CrossRef](#)]
37. Zhang, P.; Wang, K.; Wang, J.; Guo, J.; Ling, Y. Macroscopic and microscopic analyses on mechanical performance of metakaolin/fly ash based geopolymer mortar. *J. Clean. Prod.* **2021**, *294*, 126193. [[CrossRef](#)]
38. Belaabed, R.; El Knidri, H.; El Khalfaouy, R.; Addaou, A.; Laajab, A.; Lahsini, A. Zeolite Y synthesis without organic template: The effect of synthesis parameters. *J. Mater. Environ. Sci.* **2017**, *8*, 3550–3555.
39. Koshy, N.; Dondrob, K.; Hu, L.; Wen, Q.; Meegoda, J.N. Synthesis and characterization of geopolymers derived from coal gangue, fly ash and red mud. *Constr. Build. Mater.* **2019**, *206*, 287–296. [[CrossRef](#)]
40. Liu, Y.; Yan, C.; Qiu, X.; Li, D.; Wang, H.; Alshameri, A. Preparation of faujasite block from fly ash-based geopolymer via in-situ hydrothermal method. *J. Taiwan Inst. Chem. Eng.* **2016**, *76*, 433–439. [[CrossRef](#)]
41. Esteves, I.A.A.C.; Lopes, M.S.S.; Nunes, P.M.C.; Mota, J.P.B. Adsorption of natural gas and biogas components on activated carbon. *Sep. Purif. Technol.* **2008**, *62*, 281–296. [[CrossRef](#)]
42. Sayari, A.; Belmabkhout, Y. Stabilization of Amine-Containing CO<sub>2</sub> Adsorbents: Dramatic Effect of Water Vapor. *J. Am. Chem. Soc.* **2010**, *132*, 6312–6314. [[CrossRef](#)]
43. Cavenati, S.; Grande, C.A.; Rodrigues, A.E. Adsorption Equilibrium of Methane, Carbon Dioxide, and Nitrogen on Zeolite 13X at High Pressures. *J. Chem. Eng. Data* **2004**, *49*, 1095–1101. [[CrossRef](#)]

**Disclaimer/Publisher’s Note:** The statements, opinions and data contained in all publications are solely those of the individual author(s) and contributor(s) and not of MDPI and/or the editor(s). MDPI and/or the editor(s) disclaim responsibility for any injury to people or property resulting from any ideas, methods, instructions or products referred to in the content.